Statistical properties of undulator radiation in the IOTA storage ring

Ihar Lobach*
The University of Chicago, Chicago, IL 60637, USA

Valeri Lebedev, Sergei Nagaitsev,† Aleksandr Romanov, Giulio Stancari, and Alexander Valishev
Fermi National Accelerator Laboratory, Batavia, IL 60510, USA

Aliaksei Halavanau and Zhirong Huang
SLAC National Accelerator Laboratory, Stanford University, Menlo Park CA 94025, USA

Kwang-Je Kim†
Argonne National Accelerator Laboratory, Lemont, IL 60439, USA

In this paper, we study turn-by-turn fluctuations in the number of spontaneously emitted photons in an undulator, recently installed in the Integrable Optics Test Accelerator (IOTA) electron storage ring at Fermilab. We present a theoretical model, corroborated by the data from similar experiments in the past, as well as the present experiment. In our experiment, we especially consider the case of a large number of longitudinal and transverse radiation modes, and hence very small fluctuations, when the contribution from the photon shot noise becomes significant. Accordingly, we present certain critical improvements in the experimental setup, allowing the measurement of such a small value of fluctuations. In addition, we demonstrate how the attained data assist in benchmarking of the intrabeam scattering model in IOTA.

I. INTRODUCTION

In the last few decades there were several experiments regarding statistical properties of incoherent synchrotron radiation, produced by electron bunches in storage rings and linear accelerators [1–5]. ~~Namely,~~ the fluctuation in the radiated energy (or the number of photons) from pulse to pulse was studied experimentally and theoretically. It was shown in [2, 3] that in some cases the rms electron bunch length can be measured via this fluctuation. Moreover, references [4, 5] suggest that if the fluctuations in radiation spectrum are measured with a high resolution spectrometer, then even the shape of the electron bunch can be reconstructed. These ~~discoveries,~~ combined with the fact that fluctuations of the same nature are present in SASE FELs [6–11], make the fluctuations in incoherent synchrotron radiation ~~an interesting subject for further study.~~

The number of photons~~,~~ radiated incoherently by an electron bunch in an external electromagnetic field (undulator, wiggler, dipole magnet, etc.)~~,~~ fluctuates from pass to pass due to the following two mechanisms. ~~First,~~ mechanism is the photon shot noise, related to the quantum discrete nature of light. This effect would exist even if there was only one electron. Indeed, the electron would radiate light with Poisson statistics [12–14]. ~~Second~~ mechanism is that the field produced by a bunch of electrons is~~, in fact,~~ an incoherent sum of fields produced by all the electrons in the bunch. If wavepackets of radiation produced by different electrons overlap, the incoherent sum fluctuates from pass to pass because the positions of the electrons in the bunch change. In a storage ring, ~~it happens~~ because of ~~the~~ betatron motion, synchrotron motion, radiation induced diffusion, etc.; in linacs, assuming exactly equal bunch charges, ~~it happens simply because at every pass~~ there is a new bunch of electrons, positions of which are not correlated with positions of electrons in the previous bunch.

For dense bunches, the fluctuations in the number of emitted photons are usually [7] dominated by the incoherence contribution ~~and~~ it was the case in [1–5]. In this paper, we present the results of studies of statistical properties of undulator radiation in the IOTA ring at Fermilab~~, see~~ [15], where the contributions from both mechanisms are comparable. This also means that the fluctuations were very small (compared to [1], for instance), and ~~therefore,~~ we present several critical improvements to the setups from [1, 2], ~~that let us enhance accuracy.~~

We start by reviewing the theory of fluctuations in synchrotron radiation. The ~~presented~~ theory is relevant for both storage rings and linear accelerators. However, below we assume a radiation coming from a single bunch in a storage ring where the number of participating electrons does not fluctuate. We derive an equation for the variance of the number of detected photons for a Gaussian electron bunch ~~with the proper treatment of the detector quantum efficiency.~~ Then, the theoretical predictions are compared with the empirical data from [1]. Finally, we describe our experiment in IOTA [16], and how the empirical data from this experiment ~~agree~~ with our model.

* ilobach@uchicago.edu
† Also at the University of Chicago.

II. THEORETICAL MODEL

We consider incoherent synchrotron radiation (undulator, wiggler, bending-magnet, etc.), emitted by a Gaussian bunch consisting of many randomly located electrons. We assume that the synchrotron radiation is collected in a wide spectral range, and also in a large solid angle.

A. Quantum fluctuations

Even though in general we consider a bunch with randomly located electrons, in this subsection we fix positions (phases) of all the electrons and derive the quantum contribution to the fluctuations. We take the ensemble average over random positions (phases) of the electrons in subsection II B.

Conceptually, one can divide the detector into many detectors each of which senses only one mode of the produced radiation with the wavevector $\boldsymbol{k}$. The volume of the $\boldsymbol{k}$-space associated with this mode will be denoted by $d\boldsymbol{k} \equiv dk_x dk_y dk_z$. We can consider periodic boundary conditions in a cube with side L, then $d\boldsymbol{k} = (2\pi/L)^3$. We will always take the limit $L \to \infty$ at some point, and all the sums over modes $\boldsymbol{k}$ will be replaced by integrals. Upon this transition to integrals, it will also be valid to use $d\boldsymbol{k} = k^2 dk d\Omega$, where Ω is the solid angle.

It was shown in [12, 13] that any classical current (corresponding to a negligible electron recoil) produces a coherent state of radiated electromagnetic field. The coherent state in the single mode $\boldsymbol{k}$ is given by [13]

$$|\alpha_{\boldsymbol{k}}\rangle = e^{-\frac{1}{2}|\alpha_{\boldsymbol{k}}|^2} \sum_{n_{\boldsymbol{k}}} \frac{\alpha_{\boldsymbol{k}}^{n_{\boldsymbol{k}}}}{\sqrt{n_{\boldsymbol{k}}!}} |n_{\boldsymbol{k}}\rangle\,, \tag{1}$$

where $|n_{\boldsymbol{k}}\rangle$ is the state with $n_{\boldsymbol{k}}$ photons in the mode $\boldsymbol{k}$, the exact formula for $\alpha_{\boldsymbol{k}}$ is provided in [13]. For our purposes, it is sufficient to mention that

$$|\alpha_{\boldsymbol{k}}|^2 = \mathcal{N}_{\text{q.c.}}^{\boldsymbol{k},d\boldsymbol{k}} = I_{\boldsymbol{k}} d\boldsymbol{k}, \tag{2}$$

where $\mathcal{N}_{\text{q.c.}}^{\boldsymbol{k},d\boldsymbol{k}}$ is the quasi-classical number of photons emitted in mode $\boldsymbol{k}$, and $I_{\boldsymbol{k}}$ is the quasi-classical spectral-angular density of the number of emitted photons, defined in this paper by the second equality in Eq. (2). There are two perpendicular polarization components for each wavevector $\boldsymbol{k}$, usually denoted by σ and π [7]. In this paper, we omit σ and π for the sake of brevity. If there is a sum or an integral over $\boldsymbol{k}$ in any equation, it should be understood that there is a sum over both polarizations as well.

In the coherent state Eq. (1), the number of photons $n_{\boldsymbol{k}}$ obeys the Poisson statistics, so that the mean and the variance of $n_{\boldsymbol{k}}$ are equal and given by $|\alpha_{\boldsymbol{k}}|^2 = I_{\boldsymbol{k}} d\boldsymbol{k}$:

$$\langle n_{\boldsymbol{k}}\rangle = \langle\alpha_{\boldsymbol{k}}|\hat{n}_{\boldsymbol{k}}|\alpha_{\boldsymbol{k}}\rangle = |\alpha_{\boldsymbol{k}}|^2 = I_{\boldsymbol{k}} d\boldsymbol{k}, \tag{3}$$

$$\text{var}(n_{\boldsymbol{k}}) = \langle\alpha_{\boldsymbol{k}}|(\hat{n}_{\boldsymbol{k}} - \langle n_{\boldsymbol{k}}\rangle)^2|\alpha_{\boldsymbol{k}}\rangle = |\alpha_{\boldsymbol{k}}|^2 = I_{\boldsymbol{k}} d\boldsymbol{k}, \tag{4}$$

where $\hat{n}_{\boldsymbol{k}} = \hat{a}_{\boldsymbol{k}}^\dagger \hat{a}_{\boldsymbol{k}}$, with $\hat{a}_{\boldsymbol{k}}^\dagger$ and $\hat{a}_{\boldsymbol{k}}$ being the creation and annihilation operators for the mode $\boldsymbol{k}$.

A conventional approach will be used to account for the ~~($\boldsymbol{k}$-dependent)~~ quantum efficiency of the detector, $\eta_{\boldsymbol{k}}$, namely, the beam splitter model, described, for example, in [17], also see Fig. 1.

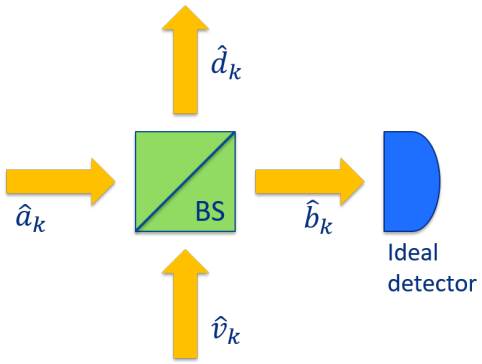

FIG. 1. The beam splitter model for quantum efficiency of a non-ideal detector.

The input-output relations for the beam splitter take the form

$$\hat{b}_{\boldsymbol{k}} = \sqrt{\eta_{\boldsymbol{k}}}\hat{a}_{\boldsymbol{k}} + i\sqrt{1-\eta_{\boldsymbol{k}}}\hat{v}_{\boldsymbol{k}}, \tag{5}$$

$$\hat{d}_{\boldsymbol{k}} = \sqrt{1-\eta_{\boldsymbol{k}}}\hat{v}_{\boldsymbol{k}} + i\sqrt{\eta_{\boldsymbol{k}}}\hat{a}_{\boldsymbol{k}}, \tag{6}$$

where $\hat{a}_{\boldsymbol{k}}$ is the incoming field, $\hat{v}_{\boldsymbol{k}}$ corresponds to the second input port, which is in the vacuum state in this model, $\hat{b}_{\boldsymbol{k}}$ and $\hat{d}_{\boldsymbol{k}}$ are transmitted and reflected fields, respectively. Equation (5) lets us calculate the mean and the variance for the number of detected photons $\mathcal{N}_{\boldsymbol{k}}$ [17]

$$\langle\mathcal{N}_{\boldsymbol{k}}\rangle = {}_{a,v}\langle\alpha_{\boldsymbol{k}},0|\hat{b}_{\boldsymbol{k}}^\dagger\hat{b}_{\boldsymbol{k}}|\alpha_{\boldsymbol{k}},0\rangle_{a,v} = \eta_{\boldsymbol{k}}\langle n_{\boldsymbol{k}}\rangle, \tag{7}$$

$$\text{var}(\mathcal{N}_{\boldsymbol{k}}) = {}_{a,v}\langle\alpha_{\boldsymbol{k}},0|(\hat{b}_{\boldsymbol{k}}^\dagger\hat{b}_{\boldsymbol{k}} - \langle\mathcal{N}_{\boldsymbol{k}}\rangle)^2|\alpha_{\boldsymbol{k}},0\rangle_{a,v} = \eta_{\boldsymbol{k}}\langle n_{\boldsymbol{k}}\rangle + \eta_{\boldsymbol{k}}^2(\text{var}(n_{\boldsymbol{k}}) - \langle n_{\boldsymbol{k}}\rangle). \tag{8}$$

In the second term in Eq. (8) one can see that it is important to have a high quantum efficiency to be able to observe the Sub- or Super-Poisson statistics [18–20] of a quantum origin. However, for coherent states this term vanishes, and, using Eqs. (3) and (4), we obtain

$$\langle\mathcal{N}_{\boldsymbol{k}}\rangle = \text{var}(\mathcal{N}_{\boldsymbol{k}}) = \eta_{\boldsymbol{k}} I_{\boldsymbol{k}} d\boldsymbol{k}. \tag{9}$$

In fact, using Eq. (5) to find how the coherent state Eq. (1) is transformed by the beam splitter, one can show that the output state will be a coherent state, and the number of detected photons $\mathcal{N}_{\boldsymbol{k}}$ will obey the Poisson statistics as well as $n_{\boldsymbol{k}}$ does. Furthermore, since a sum of independent random Poisson variables is Poissonian [21], the total number of detected photons $\mathcal{N}$,

$$\mathcal{N} = \sum_{\boldsymbol{k}} \mathcal{N}_{\boldsymbol{k}}, \tag{10}$$

will obey the Poisson distribution with the mean and the variance given by

$$\langle \mathcal{N} \rangle = \mathrm{var}(\mathcal{N}) = \int \eta_{\boldsymbol{k}} I_{\boldsymbol{k}} d\boldsymbol{k} = \mathcal{N}_{\mathrm{q.c.}}, \tag{11}$$

where $\mathcal{N}_{\mathrm{q.c.}}$ is the total number of detected photons, calculated in the quasi-classical model, the integration is performed over all $\boldsymbol{k}$, while all sources of losses can be incorporated into $\eta_{\boldsymbol{k}}$, such as the detector's quantum efficiency, losses in a focusing lens (if used), in the vacuum chamber window, finite detector's aperture ($\eta_{\boldsymbol{k}}$ can be set to zero for radiation angles that are not collected by the detector); if a spectral filter is used, its transmission function can be incorporated into $\eta_{\boldsymbol{k}}$; polarization filters can be accounted for in a similar manner.

In [14], it was shown that the total number of photons emitted (not detected) by a classical current obeys the Poisson distribution. Equation (11) is in agreement with this result, and extends it to the counts in a non-ideal detector. It is also noteworthy that for $\langle \mathcal{N} \rangle \gg 1$ the distribution for $\mathcal{N}$ is essentially Gaussian.

Equation (11) is in agreement with intuitive understanding and is usually taken for granted. In the derivations presented above, we merely reviewed the proof of Eq. (11) for the synchrotron radiation from the quantum optics perspective.

B. Classical fluctuations

Equation (11) was derived for fixed electron phases in the bunch. In actuality, in a storage ring, electrons' phases are random each turn. The number of photons, detected after one pass, can be represented as

$$\mathcal{N} = \Delta\left(\mathcal{N}_{\mathrm{q.c.}}\right) + \mathcal{N}_{\mathrm{q.c.}}, \tag{12}$$

where $\Delta\left(\mathcal{N}_{\mathrm{q.c.}}\right)$ is the random variable describing the Poisson fluctuation of the number of detected photons around the quasi-classical value $\mathcal{N}_{\mathrm{q.c.}}$, which also fluctuates from turn to turn. According to Eq. (11),

$$\langle \mathcal{N} \rangle = \mathrm{var}\left(\Delta\left(\mathcal{N}_{\mathrm{q.c.}}\right)\right) = \mathcal{N}_{\mathrm{q.c.}}. \tag{13}$$

Even though Δ is a function of $\mathcal{N}_{\mathrm{q.c.}}$, we can estimate it as $\Delta\left(\langle \mathcal{N}_{\mathrm{q.c.}} \rangle\right)$ for $\langle \mathcal{N}_{\mathrm{q.c.}} \rangle \gg 1$. Then, Δ becomes independent of $\mathcal{N}_{\mathrm{q.c.}}$ (independent of each particular instance of $\mathcal{N}_{\mathrm{q.c.}}$, but still dependent on $\langle \mathcal{N}_{\mathrm{q.c.}} \rangle$). Now, we can take variance of Eq. (12), using the fact that $\mathrm{var}(a+b) = \mathrm{var}(a) + \mathrm{var}(b)$ for independent a and b. Then, we obtain

$$\mathrm{var}(\mathcal{N}) = \mathrm{var}\left(\Delta\left(\langle \mathcal{N}_{\mathrm{q.c.}} \rangle\right)\right) + \mathrm{var}(\mathcal{N}_{\mathrm{q.c.}}). \tag{14}$$

Using Eq. (13) in Eq. (14), we obtain

$$\mathrm{var}(\mathcal{N}) = \langle \mathcal{N} \rangle + \mathrm{var}(\mathcal{N}_{\mathrm{q.c.}}). \tag{15}$$

Equation (15) can be rewritten in the form of [7, 22]

$$\mathrm{var}(\mathcal{N}) = \langle \mathcal{N} \rangle + \frac{1}{M} \langle \mathcal{N} \rangle^2, \tag{16}$$

where the parameter M was introduced. In this paper it is defined as

$$\frac{1}{M} \equiv \frac{\mathrm{var}(\mathcal{N}_{\mathrm{q.c.}})}{\langle \mathcal{N}_{\mathrm{q.c.}} \rangle^2}, \tag{17}$$

however, it is noteworthy that it can be identified with the number of coherent modes defined in [7, 23], therefore we will use this name for the parameter M from now on.

In this subsection, we find M by explicitly calculating $\mathrm{var}(\mathcal{N}_{\mathrm{q.c.}}) = \langle \mathcal{N}_{\mathrm{q.c.}}^2 \rangle - \langle \mathcal{N}_{\mathrm{q.c.}} \rangle^2$ and using Eq. (17). To begin with, we introduce $I_{\boldsymbol{k}}^{(1)}$, i.e., the quasi-classical spectral-angular density of the number of detected photons for the case when there is only one electron in the storage ring, by the following relation

$$\frac{d\mathcal{N}_{\mathrm{q.c.}}^{(1)}}{d\boldsymbol{k}} = \eta_{\boldsymbol{k}} I_{\boldsymbol{k}}^{(1)}. \tag{18}$$

Then, the total quasi-classical number of photons detected in this case is given by

$$\mathcal{N}_{\mathrm{q.c.}}^{(1)} = \int d\boldsymbol{k} \eta_{\boldsymbol{k}} I_{\boldsymbol{k}}^{(1)}. \tag{19}$$

In the derivations below, we will assume that the beam divergence is negligible compared to the radiation divergence [2, 7, 23]

$$\sigma_{x'}, \sigma_{y'} \ll \sigma_{r'}. \tag{20}$$

Also, it is assumed that the electrons' momentum spread σ_p is sufficiently small, so that all the electrons in the bunch produce radiation with approximately the same spectrum

$$\left| \frac{\partial I_{\boldsymbol{k}}^{(1)}}{\partial p} \right| \sigma_p \ll \left| I_{\boldsymbol{k}}^{(1)} \right|. \tag{21}$$

Given that conditions (20) and (21) are fulfilled (typical for an electron storage ring, [1, 2, 16]), one can use the following formula for $\mathcal{N}_{\mathrm{q.c.}}$ [2, 7, 23]

$$\mathcal{N}_{\mathrm{q.c.}} = \int d\boldsymbol{k} \eta_{\boldsymbol{k}} I_{\boldsymbol{k}}^{(1)} \left| \sum_m e^{i\boldsymbol{k}\cdot\boldsymbol{r}_m} \right|^2, \tag{22}$$

where $m = 1..N_e$, with N_e being the number of electrons in the bunch; $\boldsymbol{r}_m \equiv (x_m, y_m, -ct_m)$, x_m and y_m describe the transverse position of mth electron when it enters the synchrotron light source (undulator, wiggler, bending magnet, etc.) at time t_m. Accordingly, the square of $\mathcal{N}_{\mathrm{q.c.}}$ is given by

$$(\mathcal{N}_{\mathrm{q.c.}})^2 = \int d\boldsymbol{k}_1 d\boldsymbol{k}_2 \eta_{\boldsymbol{k}_1} I_{\boldsymbol{k}_1}^{(1)} \eta_{\boldsymbol{k}_2} I_{\boldsymbol{k}_2}^{(1)} \times \left| \sum_m e^{i\boldsymbol{k}_1\cdot\boldsymbol{r}_m} \right|^2 \left| \sum_n e^{i\boldsymbol{k}_2\cdot\boldsymbol{r}_n} \right|^2. \tag{23}$$

We consider a Gaussian distribution of particles in the bunch along x, y and ct, with rms sizes σ_x, σ_y and σ_z, respectively. The following two mathematical identities can be derived in this case

$$\langle \left| \sum_m e^{i\boldsymbol{k}\cdot\boldsymbol{r}_m} \right|^2 \rangle = N_e + N_e\,(N_e-1)\,e^{-\mathbf{K}\cdot\boldsymbol{\Sigma}}, \tag{24}$$

$$\langle \left| \sum_m e^{i\boldsymbol{k}_1\cdot\boldsymbol{r}_m} \right|^2 \left| \sum_n e^{i\boldsymbol{k}_2\cdot\boldsymbol{r}_n} \right|^2 \rangle = N_e^2 + N_e(N_e-1)e^{-\boldsymbol{\Delta}_{12}\cdot\boldsymbol{\Sigma}} + N_e(N_e-1)\left[N_e\left(e^{-\mathbf{K}_1\cdot\boldsymbol{\Sigma}}+e^{-\mathbf{K}_2\cdot\boldsymbol{\Sigma}}\right)+2\,(N_e-2)\,e^{-(\mathbf{K}_{12}+\boldsymbol{\Delta}_{12})\cdot\boldsymbol{\Sigma}}+\left(N_e^2-3N_e+3\right)e^{-(\mathbf{K}_1+\mathbf{K}_2)\cdot\boldsymbol{\Sigma}}\right], \tag{25}$$

where the average is taken over each electron's position, $\mathbf{K} \equiv (k_x^2, k_y^2, k_z^2)$ ($\mathbf{K}_1$ and $\mathbf{K}_2$ are defined analogously), $\boldsymbol{\Sigma} \equiv (\sigma_x^2, \sigma_y^2, \sigma_z^2)$, $\mathbf{K}_{12} \equiv (k_{1x}k_{2x}, k_{1y}k_{2y}, k_{1z}k_{2z})$, $\boldsymbol{\Delta}_{12} \equiv ((k_{1x}-k_{2x})^2, (k_{1y}-k_{2y})^2, (k_{1z}-k_{2z})^2)$.

In this paper, we consider radiation with sufficiently short wavelengths where contribution of coherent synchrotron radiation (CSR) is negligible. It corresponds to the condition where $k_z\sigma_z - \ln N_e \gg 1$. It is satisfied in the Brookhaven experiment [1] ($k_z\sigma_z \sim 7\times10^5$), and in our experiment [16] ($k_z\sigma_z \sim 1.2\times10^6$). Then, it is sufficient to keep only the first term in Eq. (24) and the first two terms in Eq. (25). Hence, it follows from Eqs. (22) and (24) that

$$\langle \mathcal{N}_{\text{q.c.}} \rangle = N_e \int d\boldsymbol{k}\eta_{\boldsymbol{k}} I^{(1)}_{\boldsymbol{k}} = N_e \mathcal{N}^{(1)}_{\text{q.c.}}. \tag{26}$$

Further, assuming that

$$\left| \frac{\partial I^{(1)}_{\boldsymbol{k}}}{\partial k_z} \right| \frac{1}{\sigma_z} \ll \left| I^{(1)}_{\boldsymbol{k}} \right|, \tag{27}$$

which is usually fulfilled when $k_z\sigma_z \gg 1$ (bunch length much longer than the radiation wavelength), we can use the following approximation when integrating in Eq. (23)

$$e^{-\sigma_z^2(k_{1z}-k_{2z})^2} \sim \frac{\sqrt{\pi}}{\sigma_z}\delta\left(k_{1z}-k_{2z}\right), \tag{28}$$

where $\delta\,(..)$ is the Dirac delta function.

Keeping only the first two terms in Eq. (25) and using Eq. (28) during integration in Eq. (23), and also assuming $N_e \gg 1$, we arrive at the following expression for the inverse of the number of coherent modes

$$\frac{1}{M} \equiv \frac{\mathrm{var}(\mathcal{N}_{\text{q.c.}})}{\langle \mathcal{N}_{\text{q.c.}} \rangle^2} = \frac{\frac{\sqrt{\pi}}{\sigma_z}\int dk d\Omega_1 d\Omega_2 k^4 \eta_{k\boldsymbol{n}_1} I^{(1)}_{k\boldsymbol{n}_1} \eta_{k\boldsymbol{n}_2} I^{(1)}_{k\boldsymbol{n}_2} e^{-k^2\sigma_x^2(\theta_{1x}-\theta_{2x})^2 - k^2\sigma_y^2(\theta_{1y}-\theta_{2y})^2}}{\left(\int d\boldsymbol{k}\eta_{\boldsymbol{k}} I^{(1)}_{\boldsymbol{k}}\right)^2}, \tag{29}$$

where $\boldsymbol{n}_1 \approx (\theta_{1x}, \theta_{1y}, 1)$, $\boldsymbol{n}_2 \approx (\theta_{2x}, \theta_{2y}, 1)$, i.e., it is assumed that the radiation is concentrated at small angles $\theta_x, \theta_y \lesssim 1/\gamma \ll 1$ and the paraxial approximation is used. Equation (29) is in agreement with Eq. (14) of Ref. [2]. In [2], the authors focus on the model where the electron bunch and spectral-angular distribution of the radiation is assumed to be Gaussian. In our paper, we still consider a Gaussian electron bunch, however, we do not assume the Gaussian spectral-angular distribution for the radiation in Eq. (29). Instead, we have used the expression for spectral-angular intensity distribution for the undulator radiation from Ref. [24]. In the limit of a large transverse electron bunch size, one can use approximations for x and y direction, analogous to Eq. (28), in Eq. (29) to simplify it further. In the opposite limiting case, i.e., $\sigma_x, \sigma_y \to 0$, one can omit the exponent in Eq. (29). More information on the limiting cases can be found in [2, 25]. In the numerical examples in this paper (the Brookhaven experiment [1] and our experiment [16]) we use the full version of Eq. (29) and perform numerical integration, since the values of the parameters in these experiments correspond to an intermediate case.

The assumption of Gaussian bunch works ~~great~~ in IOTA for x,x',y,y', and p. However, it fails for the distribution along z. The exact reason why is discussed in Subsection III B 3. Fortunately, Eq. (29) can still be

used, ~~given~~ that σ_z is replaced by the effective σ_z:

$$\sigma_z^{\text{eff}} = \frac{1}{2\sqrt{\pi}\int \rho^2(z)dz}, \tag{30}$$

where

$$\rho(z) \equiv \frac{1}{N_e}\frac{dN_e}{dz}. \tag{31}$$

Equation (29) does not reveal the exact distribution for $\mathcal{N}_{\text{q.c.}}$, it only gives the variance $\text{var}(\mathcal{N}_{\text{q.c.}})$. However, the form of the distribution can be suggested by a simple qualitative argument when the number of longitudinal modes M_L is much larger than one (for bending-magnet radiation $M_L \sim k_z\sigma_z$, for undulator radiation $M_L \sim k_z\sigma_z/N_u$). Indeed, in this case the total quasi-classical number of detected photons $\mathcal{N}_{\text{q.c.}}$ is a sum of a large number of independent random numbers of detected photons coming from small longitudinal ~~chunks~~ of the bunch. Therefore, according to the central limit theorem, $\mathcal{N}_{\text{q.c.}}$ must obey a normal distribution with good accuracy. More details on the exact distribution for $\mathcal{N}_{\text{q.c.}}$ can be found in [3, 7, 22, 26–28] which suggest that, in general case ~~for~~ incoherent spontaneous radiation, the quasi-classical radiated power obeys Gamma statistics.

III. COMPARISON WITH EXPERIMENTAL DATA

A. Brookhaven experiment

In the early experiment at Brookhaven National Lab [1], the fluctuations in the wiggler and bending-magnet radiation were studied at the Brookhaven~~'s~~ Vacuum-Ultraviolet Electron Storage Ring. The data in Fig. 2 were extracted from the original paper [1] by digitizing the plot. The scale was also changed from log-log to a linear scale. This procedure could have introduced some deviations from the original data, but the deviations are believed to be ~~very small~~. We did not attempt to compare the empirical data for bending-magnet radiation from [1] with our theoretical model's predictions, since the authors of [1] indicated that the data likely represented the statistical properties of the secondary photons produced in the Pyrex vacuum chamber window, rather than the statistical properties of the original bending-magnet radiation.

The data for the wiggler radiation was collected for the fundamental harmonic, $\lambda_1 = 532\,\text{nm}$. An optical interference filter with FWHM $= 3.2\,\text{nm}$ and a maximum transmission at λ_1 was used. The rms strength parameter of the wiggler was $K_w = 4$, the number of periods $N_w = 22.5$, the period length $\lambda_w = 10\,\text{cm}$. The electron beam energy was $\approx 650\,\text{MeV}$. A ~~S~~ilicon PIN photodiode was used to convert the wiggler radiation photons into photoelectrons. Two configurations of the beam optics in the vicinity of the wiggler were studied, i.e., two transverse beam profiles, tightly focused beam and loosely focused beam (see Ref. [1] and Fig. 2). The mean photoelectron count was mainly varied by using a variable neutral density filter.

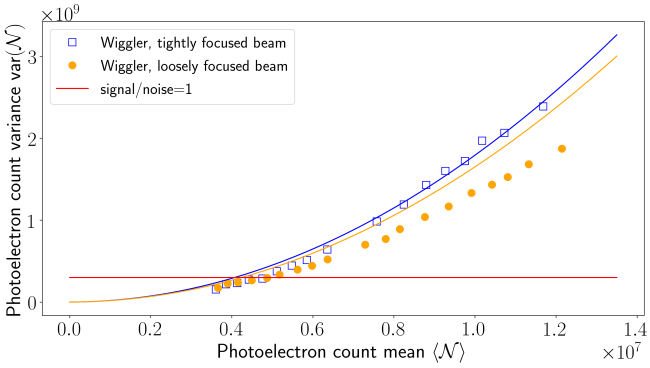

FIG. 2. Experimental data from Ref. [1] for wiggler radiation and predictions made by our theoretical model. The noise variance ($\approx 3 \times 10^8$) has been subtracted from the data.

Since the values of the photoelectron count variance $\text{var}(\mathcal{N})$ for the wiggler radiation in Fig. 2 are much larger than the values of photoelectron count mean $\langle\mathcal{N}\rangle$, it can be argued that the quantum Poisson contribution (the first term in Eq. (16)) is negligible in this experiment for the wiggler radiation. Therefore, according to our theoretical model the only remaining source of fluctuation is the incoherence contribution (the second term in Eq. (16)). We calculated it by performing numerical integration in Eq. (29) using the parameters of the electron bunch, the wiggler, and the filter, given in [1]. The Gaussian model of the filter was used. Our theoretical model, i.e., Eq. (29), predicted the following values for the number of coherent modes: for tightly focused beam, $M_{\text{TFB}} \approx 56000$; for loosely focused beam, $M_{\text{LFB}} \approx 61000$. One can see in Fig. 2 that our prediction for the tightly focused beam agrees with experimental points very well.

However, the points for the loosely focused beam deviate from our prediction. In terms of the number of coherent modes the error is about 20 % for the loosely focused beam. It is practically impossible to find the exact reason for this disagreement now, because the measurements were taken about three decades ago, and it is difficult to reconstruct the exact conditions of the experiment. In part, this is what motivated us to carry out an independent study in IOTA. Another motivation was the fact that the values of the parameters of the electron bunch and the undulator in IOTA are such that the fluctuations in the undulator radiation in IOTA are rather peculiar. In particular, the quantum and the incoherence contributions are comparable, whereas usually the latter one is dominant. Also, due to significant intrabeam scattering in IOTA, the bunch dimensions strongly depend on the beam current, and therefore, according to Eq. (29), the

dependence of the fluctuations on the beam current is nontrivial as well.

B. IOTA experiment

Integrable Optics Test Accelerator (IOTA), located at Fermilab's Accelerator Science and Technology (FAST) facility, is a small storage ring designed for experiments with both electron and proton beams. We refer the reader to Ref. [15] and Table I for the description of the ring and its parameters. In this experiment, IOTA operated with electrons only.

1. ~~Measurements setup~~

Parameters of the undulator [29] installed in IOTA, along with other essential parameters of the experiment are listed in Table I. Our photodetector~~'s~~ circuit is shown in Fig. 3. We use an InGaAs PIN photodiode (Hamamatsu G11193-10R) to convert short ($\sigma_z/c \approx 1.2\,\text{ns}$) pulses of the undulator radiation into electric current pulses of roughly the same length. Then, the current pulse quickly charges the capacitor $C_\text{f} = 2\,\text{pF}$ and the capacitor slowly ($R_\text{f}C_\text{f} = 20\,\text{ns}$) discharges through the resistor $R_\text{f} = 10\,\text{k}\Omega$, see Fig. 4. We also used the resistor $R_0 = 580\,\text{k}\Omega$ in our circuit (Fig. 3) to remove the offset in the output signal (about 300 mV) produced by the op-amp bias current and the photodiode leakage current. For this experiment, there was a single bunch in the IOTA ring, circulating with the revolution period of ~~about~~ 133 ns.

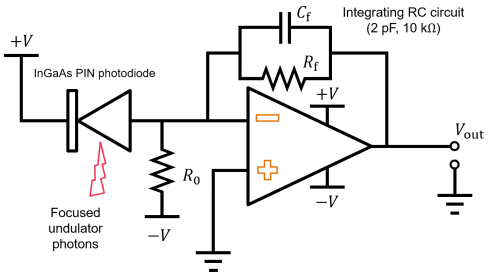

FIG. 3. A schematic of the photodetector circuit with an op-amp-based (Texas Instruments THS4304) photocurrent integrator, $V = 3.3\,\text{V}$.

TABLE I. Experimental parameters. The parameters sensitive to beam current ~~and/~~or location are given at $I_\text{beam} = 1.3\,\text{mA}$ ~~and/~~or in the center of the undulator.

IOTA circumference	40 m (133 ns)
Beam energy	100 MeV
Max average current	4.0 mA
ϵ_x, ϵ_y	0.32 μm, 31 nm
σ_p	3.1×10^{-4}
β_x, β_y	1.82 m, 1.75 m
D_x, D_y	0.87 m, 0 m
σ_x, σ_y	815 µm, 75 µm
σ_z	38 cm
Rad. damping rates $1/\tau_x$, $1/\tau_y$	$0.336\,\text{s}^{-1}$, $0.852\,\text{s}^{-1}$
$1/\tau_p$	$2.22\,\text{s}^{-1}$
Undulator parameter K_u	1.0
Undulator period	55 mm
Number of undulator periods	10
Fundamental harmonic wavelength	1077 nm
Photodiode diameter	1 mm
Quantum efficiency @1077 nm	80 %
Beam lifetime	> 10 min

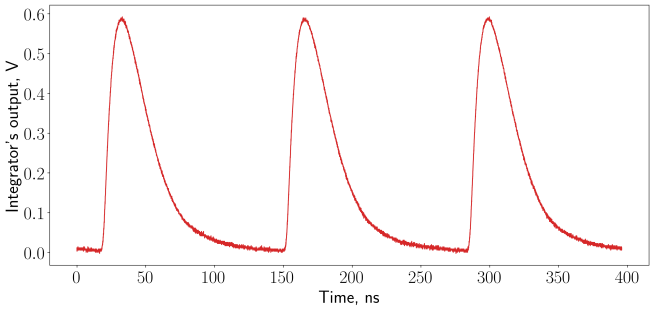

FIG. 4. Typical output of the photodiode current~~'s~~ integrator. Each pulse corresponds to one IOTA revolution.

The number of detected photons (i.e., the number of photoelectrons) is related to the voltage amplitude of the integrator~~'s~~ output signal A by

$$\mathcal{N} = \frac{C_\text{f}}{e} A, \tag{32}$$

where e is the electron charge. The amplitude A reached values up to 1.2 V during the experiment. We studied the fundamental harmonic of the undulator radiation, $\lambda_1 = 1077\,\text{nm}$. The spectrum of the fundamental was rather wide (see Fig. 5) due to the small number of periods ($N_\text{u} = 10$) in our undulator. The FEL gain length was $L_\text{g} \approx 4\,\text{m}$, while the length of the undulator was only $L_u \approx 0.6\,\text{m}$. Therefore, we observed spontaneous undulator radiation. We did not use a narrow spectral filter as in [1]. To focus the radiation on the sensitive area of the photodiode (⌀1.0 mm), we used an achromatic doublet AC508-150-C from Thorlabs (⌀2 in), so that the chromatic aberration would be minimized. The distance between the center of the undulator and the achromatic doublet was $\approx 3.5\,\text{m}$. An estimate for the collected angle is therefore $\theta_\text{ap} \approx 1\,\text{in}/3.5\,\text{m} \approx 7\,\text{mrad}$, which is comparable to $1/\gamma \approx 5\,\text{mrad}$. We believe that the actual aperture was smaller than the estimate θ_ap due to ~~using a~~ periscope with two mirrors to look at the undulator radiation ~~in IOTA~~. First, the mirrors (⌀2 in) reduce vertical aperture by a factor of $\sqrt{2}$, since they are at 45° to the direction of propagation of radiation field. Second, there could be some misalignment in the periscope. A more realistic estimate of aperture is provided in Subsec. III B 3. Nonetheless, a significant part of the undulator radia-

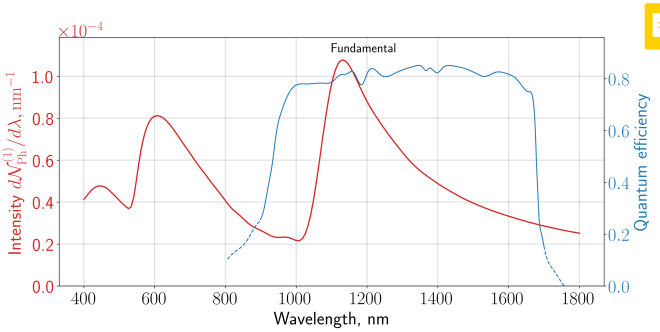

FIG. 5. Spectral density of the number of photons emitted by a single electron in the undulator into a round aperture with 2 in diameter, located 3.5 m away from the center of the undulator. The simulation was performed in SRW [30]. The quantum efficiency curve was obtained by using the photosensitivity data for the photodiode available on the Hamamatsu website [31].

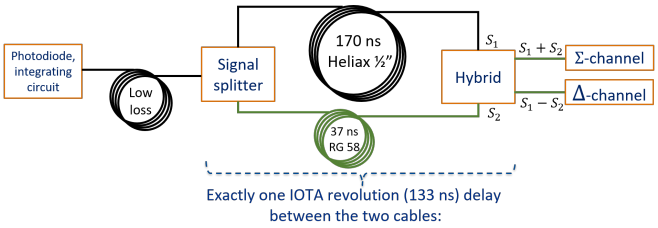

FIG. 6. A schematic of the comb filter which allows us to look directly at the amplitude difference between two consecutive pulses in IOTA (Δ-channel).

tion was collected. The photodetector was installed on a 3D-movable stage with 3 picomotors so that its position could be adjusted to maximize the collected amount of light. We also had a ~~"live"~~ video camera in our setup. Even though we could not see the fundamental harmonic with the camera, the second harmonic was in the visible part of the spectrum, and its light spot could give us an idea of where approximately the fundamental harmonic light spot was with respect to the photodiode.

It would be very hard to study small fluctuations of the amplitude ($10^{-4} - 10^{-3}$ rms) with our 8 bit ~~scope (RO-HDE&SCHWARZ~~ RTO1044 4GHz 20GSa/s) by looking directly at the integrator's output signal, see Fig. 4. To improve the ~~accuracy~~ of our measurements we use a so-called comb filter [32], see Fig. 6. The time delay between the two arms following the signal splitter equals exactly one IOTA revolution period. An adjustable phase shifter is used to fine-tune it~~, the~~ error can be made as small as a few tenths of a nanosecond. Also, the models of the cables are chosen in such a way that the losses and dispersion in the two arms are approximately the same. Then, the signals in the two arms serve as inputs to a hybrid (MACOM H-9), whose outputs are the sum and the difference of the input signals (Σ- and Δ-channels, respectively). Thus, in the Δ-channel we look directly at the difference between two consecutive IOTA pulses, i.e., the pulse-to-pulse fluctuation. When looking at the Δ-channel with a scope, all 8 bits are used effectively. Since all the elements in the comb filter are passive, practically no noise is introduced. The cross-talk between Σ- and Δ-channels was $\kappa \approx 0.7\,\%$, i.e., if the pulses in IOTA were perfectly identical, there would still be pulses in Δ-channel with amplitude of $\kappa \approx 0.7\,\%$ of the amplitude of the pulses in Σ-channel. However, this effect was easy to take into account ~~and did not downgrade the benefit of using the comb filter~~. To take one measurement of the photoelectron count variance we recorded ~~1.5 ms long~~ waveforms (~~≈~~ 11 000 IOTA revolutions) of Δ- and Σ-channels with the scope @20 GSa/sec. Since the beam lifetime in IOTA is ~~typically~~ longer than 10 min, ~~it can be easily verified that~~ the change in the number of electrons in the bunch within one waveform is negligible.

2. *Setup tests and noise subtraction*

The ability of the ~~proposed~~ setup to correctly measure the fluctuation ~~between the pulses~~ in signals similar to Fig. 4 was verified ~~in an independent measurement~~ with a test light source, which was represented by a laser diode with an amplifier modulated by a pulse generator.

One difficulty that we had to overcome in the experiment in IOTA was that the noise in Δ-channel was larger than (yet of the same order as) the turn-by-turn fluctuations in the pulses. Therefore, a special noise subtraction algorithm had to be developed and applied to the collected waveforms.

The exact procedure ~~of~~ obtaining $\mathrm{var}(\mathcal{N})$ and its uncertainty from the signals in Δ- and Σ-channels is described in Appendix, including the case of signal-to-noise ratio less than one.

3. *Measurement results for undulator radiation in IOTA and comparison with theoretical predictions*

Two sets of ~~data for the~~ undulator radiation ~~in IOTA~~ were collected. First, measurements were taken at one fixed value of beam current, 2.6 mA, and the mean photoelectron count $\langle\mathcal{N}\rangle$ was changed by placing various neutral density filters in front of the detector. We employed a four-position filter slider, which was controlled remotely. The beam was re-injected for each data point, and the measurement started when the beam current decayed to 2.6 mA. The plot of $\mathrm{var}(\mathcal{N})$ as a function of $\langle\mathcal{N}\rangle$ for this set of data is presented in Fig. 7a~~, the~~ point with maximum $\langle\mathcal{N}\rangle$ represents the ~~no-filter~~ configuration. The blue dashed curve is a fit of the form of Eq. (16) for the experimental points, $M_{\rm fit} = 3.0 \times 10^6$. In the second set of data, we did not use any neutral density filters, the mean photoelectron count $\langle\mathcal{N}\rangle$ was varied by changing the electron bunch charge, see Fig. 7b. The beam was re-injected several times, and every time multiple data

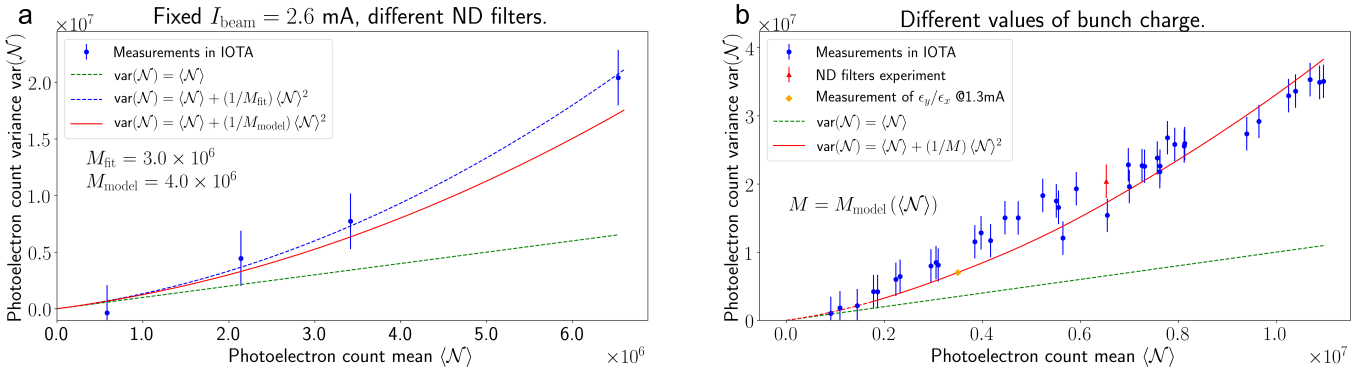

FIG. 7. Photoelectron count variance $\mathrm{var}(\mathcal{N})$ as a function of photoelectron count mean $\langle\mathcal{N}\rangle$ for undulator radiation in IOTA. (a) $\langle\mathcal{N}\rangle$ was varied by using different neutral density (ND) filters, (b) $\langle\mathcal{N}\rangle$ was varied by changing the number of electrons in the bunch. The error bar is constant and equals 2.5×10^6, see Appendix.

points were collected as the current slowly decayed. The red triangle data point is the no-filter point from Fig. 7a. The green dashed straight lines in Fig. 7a,b represent the predicted Poisson contribution.

To make a theoretical prediction for M and, consequently, for $\mathrm{var}(\mathcal{N})$, we had to know the dimensions of the electron bunch in IOTA as a function of bunch charge. To be able to estimate the bunch dimensions for the range of beam current values in our experiments, we developed a theoretical model of bunch evolution, including several effects and consistent with the available experimental data.

In addition to synchrotron radiation damping and radiation diffusion, there are three main effects, determining the bunch parameters in IOTA, namely, intrabeam scattering [33], multiple Coulomb scattering in the background gas [34], and longitudinal bunch self-focusing [35] due to space-charge. We use the method described in [33, 36] to compute emittance growth rates associated with intrabeam scattering. Let us define the intrabeam scattering growth rates in momentum p, in the horizontal x, and in the vertical y directions as

$$\frac{1}{T_p} = \frac{1}{\sigma_p^2}\frac{d\sigma_p^2}{dt}, \quad \frac{1}{T_x} = \frac{1}{\epsilon_x}\frac{d\epsilon_x}{dt}, \quad \frac{1}{T_y} = \frac{1}{\epsilon_y}\frac{d\epsilon_y}{dt}, \tag{33}$$

In our simulations, we keep the longitudinal bunch size constant, $\sigma_z = 38\,\mathrm{cm}$. This value was determined experimentally with a wall-current monitor and it remained approximately constant for any $I_{\rm beam} > 0.65\,\mathrm{mA}$. Most likely, this is due to the above mentioned self-focusing of the electron bunch in IOTA. The self-focusing also causes some deviations from Gaussian longitudinal bunch profile. However, ~~fortunately~~ Eq. (29) can still be used if one substitutes σ_z with $\sigma_z^{\rm eff}$, see Eq. (30). ~~Regardless of the exact reason why the longitudinal bunch size was constant, we will use it as an empirical fact.~~ Since in our model we assume one specific constant value of $\sigma_z = 38\,\mathrm{cm}$, it will be valid only for $I_{\rm beam} > 0.65\,\mathrm{mA}$ ($\langle\mathcal{N}\rangle > 1.75 \times 10^6$).

The horizontal and vertical betatron tunes were decoupled and linear coupling was minimized ~~for our experimental settings~~. ~~By making some preliminary estimations of intrabeam scattering growth rates, we noticed that for reasonable~~ bunch dimensions, the intrabeam scattering growth rate ~~for~~ y-direction is much smaller than the synchrotron radiation damping rate [37]. Therefore, ~~we believe that~~ vertical emittance is primarily determined by multiple Coulomb scattering ~~in~~ the residual gas. Moreover, this implies that vertical emittance ϵ_y, and, consequently, vertical bunch size σ_y do not depend on beam current.

In x-direction, the horizontal rms emittance at zero beam current, determined by quantum fluctuations, ~~would be~~ $\epsilon_{x0} = 3.6 \times 10^{-2}\,\mu\mathrm{m}$. The contribution from multiple Coulomb scattering ~~would be~~ negligible compared to that from quantum fluctuations. For $I_{\rm beam} > 0.65\,\mathrm{mA}$, both the contribution from quantum fluctuations, and the contribution from multiple Coulomb scattering are negligible compared to the intrabeam scattering growth rate (it will be shown quantitatively below), and, hence, horizontal emittance ϵ_x is defined solely by the balance between the synchrotron radiation damping rate $1/\tau_x$ (see Table I) and the intrabeam scattering growth rate $(1/T_x)$:

$$\frac{1}{\tau_x} = \frac{1}{T_x}. \tag{34}$$

In the longitudinal direction, the contribution from quantum fluctuations could in principle be neglected, since it was about one order of magnitude smaller than that from intrabeam scattering, but it was not difficult to account for it [38], therefore it was taken into consideration. Thus, the rms momentum spread σ_p was ~~defined~~ by the balance between synchrotron radiation damping on one side and intrabeam scattering growth rate and quantum fluctuations on the other side:

$$\frac{\sigma_p^2}{\tau_p} = \frac{\sigma_p^2}{T_p} + \frac{\sigma_{p0}^2}{\tau_p}, \tag{35}$$

where $\sigma_{p0} = 8.4 \times 10^{-5}$ is the momentum spread due

to synchrotron radiation alone, in the absence of intrabeam scattering; $1/\tau_p$ is the synchrotron radiation damping rate, see Table I.

At this point in our analysis, we have three unknowns, namely, ϵ_x, ϵ_y, σ_p and only two equations, i.e., Eqs. (34) and (35). We do not have an equation for y-direction, since we do not know the exact composition of the background gas.

To resolve this uncertainty, we ~~have~~ recorded several optical images of dipole-magnet synchrotron radiation from a circulating bunch at $I_{\rm beam} = 1.3\,$mA ~~and it was possible to determine the ratio of transverse emittances from these images and from the known betatron and dispersion functions~~, $\epsilon_y/\epsilon_x = 9.5\times10^{-2}$. Given this constraint, we had two equations and two unknowns at $I_{\rm beam} = 1.3\,$mA. Therefore, we were able to find all the parameters of the bunch at this value of beam current, $\epsilon_x = 0.32\,\mu$m, $\epsilon_y = 31\,$nm, $\sigma_p = 3.1\times10^{-4}$, $\sigma_x = 815\,\mu$m, $\sigma_y = 75\,\mu$m, $\sigma_z = 38\,$cm. These are the values given in Table I. This value of the beam current is marked by an orange diamond in Fig. 7b and by a green vertical line in Fig. 8.

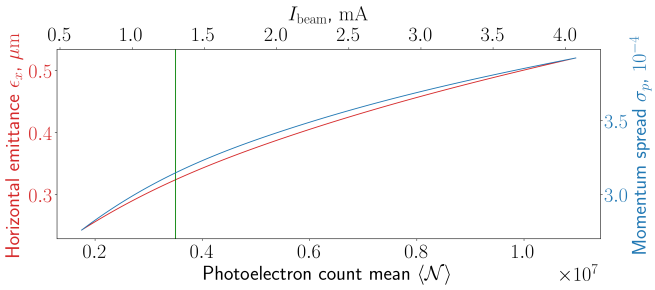

FIG. 8. Results of simulations of intrabeam scattering in IOTA. Horizontal emittance, and momentum spread in IOTA as functions of beam current $I_{\rm beam}$ and mean photoelectron count $\langle\mathcal{N}\rangle$. The green vertical ~~lines indicate~~ the beam current value 1.3 mA, at which we measured the ratio of transverse emittances by looking at the ~~pictures~~ of bending-magnet radiation.

As was mentioned above, we believe that the vertical emittance does not depend on the beam current. Therefore, we could use the value of $\epsilon_y = 31\,$nm found at $I_{\rm beam} = 1.3\,$mA for other values of the beam current. Hence, at this point, at other values of the beam current we had two unknowns, ϵ_x and σ_p, and two equations, Eqs. (34) and (35). Thus, we were able to compute ϵ_x and σ_p (see Fig. 8), and, consequently, all parameters of the bunch for all current values $I_{\rm beam} > 0.65\,$mA. Finally, Eq. (29) was used to compute M for all values of beam current $I_{\rm beam} > 0.65\,$mA, and Eq. (16) to plot the theoretical red solid curves in Fig. 7a,b. However, it should be noted that there is some uncertainty in the ~~number of parameters in IOTA~~ and in the geometry of undulator radiation detection. For most parameters we estimate this uncertainty to be $\pm10-20\%$. ~~For example, we did not know the exact angular range collected by the detector.~~ The aperture that we used in our simulations was elliptical with horizontal semi-axis equal to 3.0 mrad, and vertical semi-axis equal to 2.2 mrad. ~~We must point out, the red solid curves in Fig. 7 a,b should be understood as our best estimate, rather than an absolute theoretical prediction.~~ ~~Note that in~~ Fig. 7b, the part of the red curve for small values of the beam current $I_{\rm beam} < 0.65\,$mA is depicted by a dashed curve, indicating that our assumption of constant σ_z is altered in this region.

4. *Discussion*

~~The agreement between the theoretical model (red solid curves) and the experimental points in Fig. 7a,b is fairly good.~~ ~~It is noteworthy that in~~ Fig. 7a the parameter M is constant. ~~Indeed,~~ since the measurements are taken at one specific value of beam current, the dimensions of the electron bunch are also the same during measurements with different neutral density filters. Therefore, the M parameter must also stay the same~~,~~ ~~and the~~ red solid curve ~~(or~~ the blue dashed curve~~)~~ in Fig. 7a ~~is a parabola~~ of the form of Eq. (16) with a fixed M.

However, in Fig. 7b, the M parameter changes significantly, i.e., from $M = 3.5\times10^6$ at $\langle\mathcal{N}\rangle = 3.5\times10^6$, to $M = 4.4\times10^6$ at $\langle\mathcal{N}\rangle = 1.1\times10^7$, due to the changes in bunch dimensions. Thus, the red solid curve in Fig. 7b is no longer a parabola. ~~This actually points out~~ one possible application ~~of our analysis~~, namely, estimating the bunch dimensions by looking at the fluctuations in synchrotron radiation in a storage ring. Clearly, in general, the amplitude of fluctuations depends on all three bunch sizes, σ_x, σ_y, σ_z. Nonetheless, in some cases additional constraints or relations may be available. For example, the ratio of transverse emittances may be known; or some ~~of~~ bunch dimensions may be ~~measured more easily~~, e.g., if σ_z ~~is large (in IOTA)~~, it can be readily measured with a wall-current monitor. The ~~proposed~~ method of estimating the bunch dimensions by measuring the fluctuations in synchrotron radiation may be especially useful when one of the bunch dimensions is very small, and it is difficult to measure it with conventional methods. Successful measurements of longitudinal bunch size with this technique were reported in [2, 3]. Moreover, if fluctuations data are available in a wide spectral range, the longitudinal bunch profile may be reconstructed [4, 5]. However, it should be understood that for this method to work the radiation must be incoherent, i.e., in order to measure σ_z, the wavelength of the radiation should be significantly smaller than σ_z. In the opposite limit, M_L ~~would be~~ equal to one, and the fluctuations ~~would be~~ insensitive to σ_z.

In Fig. 7a,b, one can see that the Poisson contribution (green dashed line) is comparable with the incoherence contribution (second term in Eq. (16)). Usually the incoherence contribution is dominant [7]. There are several reasons why the two terms in Eq. (16) were comparable

in IOTA, ~~namely,~~ the small number of undulator periods $N_u = 10$, a relatively small undulator parameter $K_u = 1$, a relatively low beam current $I_{\rm beam} \lessapprox 4\,{\rm mA}$ (which means small $\langle\mathcal{N}\rangle$); a relatively large $\sigma_z = 38\,{\rm cm}$ (which means large M_L). To ~~the best of~~ our knowledge, ~~our~~ experiment in IOTA is the only ~~experiment~~ where the Poisson contribution was significant in ~~the~~ undulator radiation, as opposed to [1, 3–5], for example. However, in ~~a~~ bending-magnet radiation a situation similar to ours (with a considerable Poisson term) was observed in [2].

IV. CONCLUSIONS AND ~~FUTURE~~ OUTLOOK

We derived ~~Eqs. (16) and (29),~~ ~~which can~~ predict the fluctuations $\mathrm{var}(\mathcal{N})$ in the incoherent synchrotron ~~(undulator, wiggler, bending-magnet, etc.)~~ radiation for a Gaussian electron bunch. ~~They~~ properly take into account the ~~quantum~~ discrete nature of light and the quantum efficiency of the detector, which ~~can be~~ a function of the radiation wavelength. A spectral filter with any transmission function can be incorporated by including a transmission function into $\eta_{\boldsymbol{k}}$ in Eq. (29). The ~~radiation in arbitrary angular range~~ can be ~~considered~~ by setting $\eta_{\boldsymbol{k}}$ to zero outside ~~of that~~ range.

The ~~predictions made by our model were~~ compared with the empirical data from [1] for the case of wiggler radiation with dominant incoherence contribution and with ~~the~~ experimental data from IOTA for the case of comparable quantum and incoherence contributions. ~~In both cases, the agreement was fairly good.~~ In [1], the photoelectron count mean $\langle\mathcal{N}\rangle$ was varied mainly by using different neutral density filters. In our experiment, in addition to varying $\langle\mathcal{N}\rangle$ with different neutral density filters, we also varied $\langle\mathcal{N}\rangle$ by changing the beam current in a wide range. The latter set of data ~~helped refining~~ the model of intrabeam scattering in IOTA.

The fact that the quantum Poisson contribution to fluctuations was significant in IOTA ~~also implies~~ the value of fluctuations ~~to be~~ very small, ~~e.g.,~~ two orders of magnitude smaller than in [1]. Accordingly, we introduced several critical improvements to the experimental setup that dramatically increased the ~~accuracy of measurements~~. In particular, we used ~~the~~ comb filter with a delay equal to one IOTA revolution, and ~~the~~ special noise ~~subtraction~~ algorithm.

~~In general, we believe that Eqs. (16) and (29) can provide a prediction that will agree with experimental results within a few percent.~~ In our present experimental configuration, the ~~uncertainty in~~ electron bunch size, undulator radiation direction, and ~~some parameters of~~ the photodetector's circuit were the main sources ~~of discrepancy with the theory and altered the final result~~. ~~However, we believe, with better diagnostics, we will achieve much better agreement in the future.~~

~~We can conclude that the best way to benchmark our theoretical model against experimental results~~ is to collect the fluctuations data at fixed beam current, as in Fig. 7a. In this case, the parameter M is constant, and provides an indirect measurement of the bunch dimensions.

In ~~addition, as another verification of our model~~, we plan to use a larger electron bunch (larger M) and consider the case ~~when~~ the quantum Poisson contribution is dominant, i.e., to observe the green dashed line in Fig. 7a,b experimentally.

~~As Refs. [2–5] pointed out~~, the fluctuations in synchrotron radiation can be used to make measurements of the bunch length on a picosecond scale, and the proof of principle experiments were successful. ~~It is noteworthy that~~ in IOTA, the longitudinal bunch size is relatively large $\sigma_z \approx 38\,{\rm cm}$ and can be easily measured with a wall-current monitor. ~~Whereas~~ transverse bunch size can be ~~made~~ quite small, down to a few tens of microns, ~~when~~ it may be hard to measure by conventional methods. ~~Yet~~ the number of coherent modes M in undulator radiation in IOTA is very sensitive to the transverse bunch size. Therefore, the transverse bunch dimensions ~~are still imprinted in~~ the ~~fluctuation of~~ the number of photoelectrons ~~produced in the detector and can be deduced from var$(\mathcal{N})$~~ .

ACKNOWLEDGMENTS

We would like to thank the entire FAST/IOTA team for helping us with building and installing the ~~presented setup, and taking measurements~~, especially Wayne Johnson, Mark Obrycki, and James Santucci. We also thank Greg Saewert for constructing the photodetector circuit and providing the test light source, David Johnson and Todd Johnson ~~for kindly providing~~ test equipment and ~~assisting during tests of our detector~~. Numerous pieces of advice given by Daniil Frolov are greatly appreciated as well. Finally, A.H. is grateful to C. Pellegrini, G. Stupakov and Y. Cai (SLAC) for many in-depth physics discussions on the subject.

This research is supported by the University of Chicago and the US Department of Energy under contracts ~~No. DE-AC02-07CH11359,~~ DE-AC02-76SF00515 and DE-AC02-06CH11357.

Appendix A: Setup tests and noise subtraction

The setup was tested with a test light source, which consisted of a laser diode (1064 nm) with an amplifier, modulated by a pulse generator. We also varied the mean photoelectron count (and photoelectron count variance) by putting different neutral density filters in front of the test light source. We believe that the fluctuations in the number of emitted photons in the test light source were mostly created by the jitter in the pulse generator. ~~We did not know the exact~~ value of $\mathrm{var}(\mathcal{N})$ in the test light source ~~initially, it~~ was determined with our setup. A typical waveform for Δ- and Σ-channels for the test

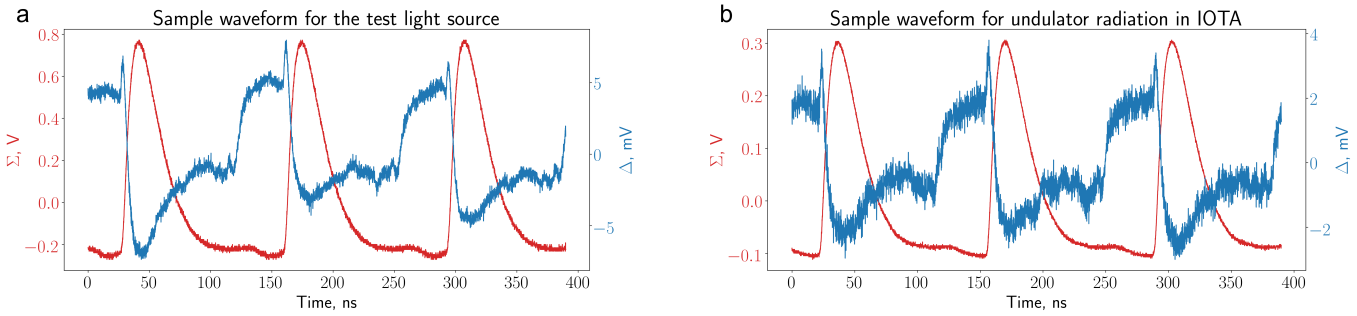

FIG. 9. (a) Sample ~~waveform~~ for the test light source without any neutral density filters, $\langle\mathcal{N}\rangle = 1.8\times10^7$, $\mathrm{var}(\mathcal{N}) = 1.1\times10^9$, signal/noise$\gg 1$; (b) Typical waveform for the undulator radiation in IOTA, $\langle\mathcal{N}\rangle = 0.73\times10^7$, $\mathrm{var}(\mathcal{N}) = 2.3\times10^7$.

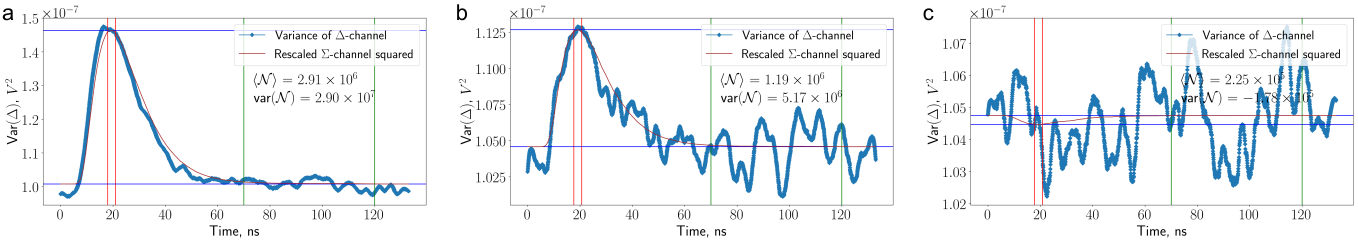

FIG. 10. ~~Application examples~~ of the noise ~~subtraction~~ algorithm for the test light source with different neutral density filters. (a) var(Δ) takes the expected shape, i.e., a peak on top of a constant level; (b) Smaller fluctuations of Δ, the peak is not as well defined as before; (c) Very small fluctuations of Δ, the peak cannot be seen in the noise.

light source without any neutral density filters is shown in Fig. 9a. The ~~jumps~~ in Δ- and Σ-signals at $\sim$ ~~100~~ ns after the main peaks are ~~most~~ likely produced by imperfection of the hybrid, which is designed to work at frequencies between 2 MHz and 2 GHz~~, whereas the~~ IOTA pulses come at 7.5 MHz, which is ~~rather~~ close to the lower limit of the hybrid. The signal ~~in~~ the integrator~~'s~~ output does not ~~have these jumps~~, see Fig. 4.

One can see in Fig. 9a that the comb filter technique works rather well. The amplitudes of the pulses in Δ-channel fluctuate significantly from pulse to pulse. And the range of these fluctuations is much larger than the noise in Δ-channel. Therefore, by analyzing these fluctuations for $\sim$ 11 000 periods, the relative fluctuation of photoelectron count for the test light source was quite reliably determined to be $\theta \equiv \mathrm{var}(\mathcal{N})/\langle\mathcal{N}\rangle^2 = 3.35\times10^{-6}$.

However, in the actual experiment with the undulator radiation in IOTA, the fluctuations in the pulse amplitudes in the Δ-channel were smaller than for the test light source, see Fig. 9b. Moreover, they were smaller than the noise in Δ-channel. Therefore, it was necessary to develop a method to ~~subtract~~ the instrumental noise and extract the actual fluctuations of the photoelectron count. The idea of the method is the following. The signal in Δ-channel is given by

$$\Delta(t) = (\delta_2 - \delta_1)\Sigma(t) + \kappa\Sigma(t) + \text{noise}, \qquad \text{(A1)}$$

where δ_1 and δ_2 describe the fluctuations in two consecutive pulses, the second term represents the cross-talk between Σ- and Δ-channels, and the last term represents any linear uniform with time noise in Δ-channel. Equation (A1) implicitly uses the fact that the fluctuations of $\Sigma(t)$ are small from pulse to pulse. In fact, from now on we will treat $\Sigma(t)$ as if it is the same every turn. If we freeze the time t in Eq. (A1) and take variance on both sides of the equation, then we obtain

$$\mathrm{var}(\Delta(t)) = 2\mathrm{var}(\delta)\Sigma^2(t) + \mathrm{var}(\text{noise}), \qquad \text{(A2)}$$

where we take into account the fact that for two independent random variables δ_1 and δ_2, the following equation is correct

$$\mathrm{var}(\delta_2 - \delta_1) = \mathrm{var}(\delta_1) + \mathrm{var}(\delta_2), \qquad \text{(A3)}$$

and, since the two terms on the right-hand side of Eq. (A3) are equal, one can replace them with $2\mathrm{var}(\delta)$. The variance of noise in Eq. (A2) is a constant, given that the noise rms amplitude is uniform with time. Therefore, $\mathrm{var}(\Delta(t))$ as a function of time is a peak with a maximum value proportional to $\Sigma^2(t)$ on top of a certain constant level offset, determined by var(noise) (see Fig. 10). The value of $\mathrm{var}(\delta)$ can be extracted from the height of this peak using Eq. (A2), and, therefore, $\mathrm{var}(\mathcal{N})$ can be found. ~~Fortunately, it is possible to~~ plot $\mathrm{var}(\Delta(t))$ ~~with~~ the empirical data that we collected (waveforms with $\sim$ 11000 ~~pulses~~). First, we analyze the Σ-channel to determine the period with which the pulses arrive with very high ~~accuracy~~ (> 7 significant figures). In IOTA, it is the revolution time (133 ns); in the test light source, it is the period in the pulse generator, which was chosen

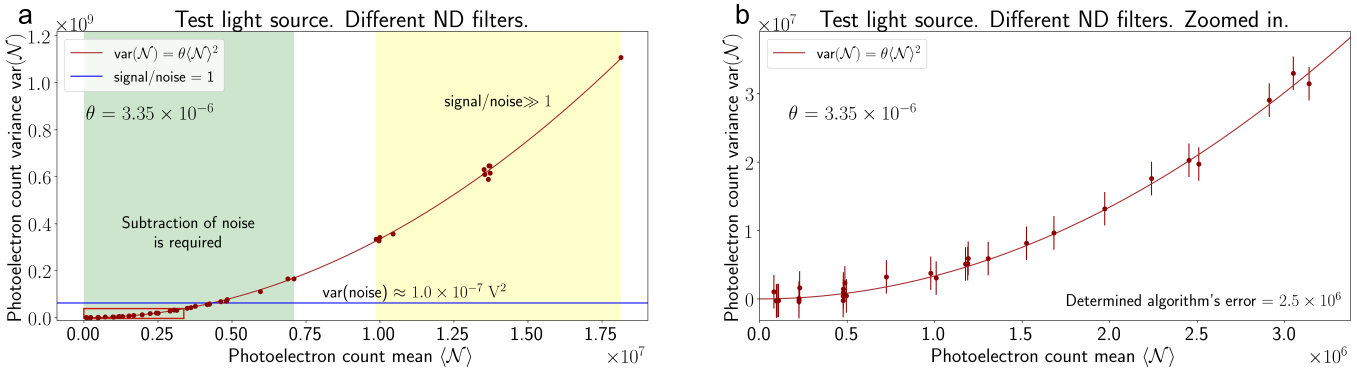

FIG. 11. Photoelectron count variance var($\mathcal{N}$) as a function of photoelectron count mean $\langle\mathcal{N}\rangle$ for the test light source, $\langle\mathcal{N}\rangle$ was varied by using different neutral density (ND) filters. (a) Entire considered range of $\langle\mathcal{N}\rangle$; (b) The region corresponding to the actual values of var($\mathcal{N}$) in the undulator radiation in IOTA (highlighted by the red rectangle in (a)).

to be 133 ns as well. Then, all the data in Δ-channel are mapped onto a single period. Further, these data are binned along the time axis into ≈ ~~2650 bins~~. Lastly, the variance of $\Delta(t)$ is calculated in each of these bins. Examples of the result of this procedure are given in Fig. 10, where the light from the test light source, significantly attenuated by neutral density filters, is studied. In this case, the signal-to-noise ratio is less than one, just like for the undulator radiation in IOTA ~~(more details on this will be given below)~~.

In Fig. 10a, we can see that the empirical var($\Delta(t)$) indeed takes the expected shape, i.e., a peak on top of a constant offset. In Fig. 10b, the case of smaller fluctuations of Δ is considered, and, the peak is not as well defined as in Fig. 10a~~, but the method still works reasonably well~~. In Fig. 10c, the case of very small fluctuations of Δ is considered, and the peak cannot be ~~found in the noise at all~~. The height of the peaks is calculated as the difference between the averages in the region between the red vertical lines (~~maximum of~~ ~~$\Sigma^2(t)$~~), and in the region between the green vertical lines. Therefore, it can be seen in Fig. 10c, that the method may mistakenly yield a slightly negative value for var($\mathcal{N}$) for very small fluctuations. ~~However, clearly, when the confidence interval is calculated for each measurement, it will always include some positive region for var($\mathcal{N}$). The exact value of error bar will be determined below.~~ ~~It is noteworthy that in~~ all three plots in Fig. 10 the constant var(~~noise~~) is approximately the same ~~≈~~ $1.0 \times 10^{-7}\,\mathrm{V}^2$, which supports the ~~claim that the method works well~~.

This method to determine the height of the peak (calculating the difference between the averages in the region between the red vertical lines (maximum of $\Sigma^2(t)$), and in the region between the green vertical lines) was chosen, because it is believed to be insensitive to small errors in the delay in the comb filter and small variations in the period with which the pulses arrive. Determining the height, by, for example, fitting the peak with $\Sigma^2(t)$ would be sensitive to these errors, because they introduce some deviations of the peak shape from $\Sigma^2(t)$. However, these deviations vanish at the maximum of the peak, where $\Sigma'(t) = 0$. This is why looking at the value of var($\Delta(t)$) at the maximum of $\Sigma(t)$ is believed to be more reliable.

The ~~described method of noise subtraction~~ was tested with the test light source. We placed various neutral density filters in front of the test light source and measured var($\mathcal{N}$) as a function of $\langle\mathcal{N}\rangle$, see Fig. 11a.

When the light was not attenuated at all, or only slightly attenuated by neutral density filters, the signal-to-noise ratio was much larger than one and var($\mathcal{N}$) could be determined directly by looking at the Δ-channel waveform without using the noise ~~subtraction~~ algorithm. ~~Moreover, by~~ repeating this measurement many times for the same neutral density filter we made sure that var($\mathcal{N}$) ~~is~~ stable in time for the test light source, see the group of points around $\langle N\rangle = 1.3 \times 10^7$ in Fig. 11a.

When the light intensity was reduced further ~~by using neutral density filters with higher optical density~~, the contribution from noise became substantial, and we had to use the ~~developed noise subtraction~~ method to measure var($\mathcal{N}$). However, we could also independently predict var($\mathcal{N}$) based on the measurements of fluctuations in the region where signal/noise$\gg 1$. ~~Indeed, when~~ quantum Poisson fluctuation can be neglected, the variance of number of photoelectrons var($\mathcal{N}$) scales as η^2, and the mean photoelectron count $\langle\mathcal{N}\rangle$ scales as η, where η is the attenuation factor of the neutral density filter. Therefore, the relative fluctuation remains constant

$$\theta \equiv \frac{\mathrm{var}(\mathcal{N})}{\langle\mathcal{N}\rangle^2} = const. \tag{A4}$$

~~Quantum~~ Poisson contribution to the fluctuations in the test light source pulses could be completely neglected, because var($\mathcal{N}$) ~~is~~ much larger than $\langle\mathcal{N}\rangle$ in Fig. 11a,b, i.e., the fluctuations ~~are~~ dominated by the generator's pulse-to-pulse amplitude jitter.

From the points with signal/noise$\gg 1$ (see Fig. 11a) it was determined that $\theta = 3.35 \times 10^{-6}$. The parabola defined by Eq. (A4) with this value of θ is plotted in Fig. 11a,b, solid line. It can be seen in Fig. 11a, and,

especially, in Fig. 11b, that the points, obtained with the noise subtraction algorithm in the region where the contribution of noise is significant, ~~agree very well with~~ the predicted parabola. In Fig. 11b, ~~the region~~ of var($\mathcal{N}$), similar to the ~~actual~~ experiment with ~~the~~ undulator radiation in IOTA~~, is presented~~. The agreement in this plot ~~proves~~ that the noise subtraction algorithm works well in the ~~experiment in IOTA~~. Three standard deviations of the points in Fig. 11b from the predicted parabola are used as the error bar for the data obtained for the undulator radiation in IOTA. The error bar equals 2.5×10^6. It is also used in Fig. 11b.

~~To summarize the results of this test, the described noise subtraction~~ algorithm can remove any linear uniform in time ~~noise~~. By linear, we mean that the noise enters in Eq. (A1) as a summand ~~term~~, independent on the amplitude of the actual Δ or Σ pulses. Sources of such contributions to noise are, for example, oscilloscope, integrator~~'s~~ op-amp, photodiode, ~~some~~ external noise sources. However, it is important to emphasize that the ~~tests~~ with the test light source were performed in a lab, not in the IOTA ring enclosure. Therefore, we cannot completely eliminate the possibility that in the IOTA ring enclosure the results of our measurements were affected by some sources of nonlinear time-dependent noise.

[1] M. C. Teich, T. Tanabe, T. C. Marshall, and J. Galayda, Statistical properties of wiggler and bending-magnet radiation from the Brookhaven Vacuum-Ultraviolet electron storage ring, Phys. Rev. Lett. **65**, 3393 (1990).

[2] F. Sannibale, G. Stupakov, M. Zolotorev, D. Filippetto, and L. Jägerhofer, Absolute bunch length measurements by incoherent radiation fluctuation analysis, Phys. Rev. ST Accel. Beams **12**, 032801 (2009).

[3] P. Catravas, W. Leemans, J. Wurtele, M. Zolotorev, M. Babzien, I. Ben-Zvi, Z. Segalov, X.-J. Wang, and V. Yakimenko, Measurement of electron-beam bunch length and emittance using shot-noise-driven fluctuations in incoherent radiation, Phys. Rev. Lett. **82**, 5261 (1999).

[4] V. Sajaev, Measurement of bunch length using spectral analysis of incoherent radiation fluctuations, in *AIP Conf. Proc.*, Vol. 732 (AIP, 2004) pp. 73–87.

[5] V. Sajaev, *Determination of longitudinal bunch profile using spectral fluctuations of incoherent radiation*, Report No ANL/ASD/CP-100935 (Argonne National Laboratory, 2000).

[6] K.-J. Kim, Start-up noise in 3-D self-amplified spontaneous emission, Nucl. Instrum. Methods Phys. Res., Sect. A **393**, 167 (1997).

[7] K.-J. Kim, Z. Huang, and R. Lindberg, *Synchrotron radiation and free-electron lasers* (Cambridge University Press, 2017).

[8] S. Benson and J. M. Madey, Shot and quantum noise in free electron lasers, Nucl. Instrum. Methods Phys. Res., Sect. A **237**, 55 (1985).

[9] E. L. Saldin, E. Schneidmiller, and M. V. Yurkov, *The physics of free electron lasers* (Springer Science & Business Media, 2013).

[10] C. Pellegrini, A. Marinelli, and S. Reiche, The physics of x-ray free-electron lasers, Rev. Mod. Phys. **88**, 015006 (2016).

[11] W. Beckerand M. S. Zubairy, Photon statistics of a free-electron laser, Phys. Rev. A **25**, 2200 (1982).

[12] R. J. Glauber, The quantum theory of optical coherence, Phys. Rev. **130**, 2529 (1963).

[13] R. J. Glauber, Coherent and incoherent states of the radiation field, Phys. Rev. **131**, 2766 (1963).

[14] R. J. Glauber, Some notes on multiple-boson processes, Phys. Rev. **84**, 395 (1951).

[15] S. Antipov, D. Broemmelsiek, D. Bruhwiler, D. Edstrom, E. Harms, V. Lebedev, J. Leibfritz, S. Nagaitsev, C.-S. Park, H. Piekarz, *et al.*, IOTA (Integrable Optics Test Accelerator): facility and experimental beam physics program, J. Instrum. **12** (03), T03002.

[16] I. Lobach, K.-J. Kim, T. Shaftan, V. Lebedev, S. Nagaitsev, A. Romanov, G. Stancari, A. Valishev, A. Murokh, A. Halavanau, Z. Huang, and V. Yakimenko, Study of Fluctuations in Undulator Radiation in the IOTA Ring at Fermilab, in *Proc. 10th International Partile Accelerator Conference (IPAC'19), Melbourne, Australia, 19-24 May 2019*, 10 (2019) pp. 777–780.

[17] A. Meda, E. Losero, N. Samantaray, F. Scafirimuto, S. Pradyumna, A. Avella, I. Ruo-Berchera, and M. Genovese, Photon-number correlation for quantum enhanced imaging and sensing, J. Opt. **19**, 094002 (2017).

[18] T. Chen, *Photon statistics of coherent harmonic radiation of a linac free electron laser*, Ph.D. thesis, Duke University (1999).

[19] T. Chen and J. M. Madey, Observation of sub-Poisson fluctuations in the intensity of the seventh coherent spontaneous harmonic emitted by a RF linac free-electron laser, Phys. Rev. Lett. **86**, 5906 (2001).

[20] J. M. Madey, Wilson Prize article: From vacuum tubes to lasers and back again, Phys. Rev. ST Accel. Beams **17**, 074901 (2014).

[21] G. Grimmett and D. Welsh, *Probability: an introduction* (Oxford University Press, 2014).

[22] K.-J. Kim, Temporal and transverse coherence of self-amplified spontaneous emission, in *AIP Conf. Proc.*, Vol. 413 (AIP, 1997) pp. 3–13.

[23] K.-J. Kim, Characteristics of synchrotron radiation, in *AIP Conf. Proc.*, Vol. 184 (AIP, 1989) pp. 565–632.

[24] J. A. Clarke, *The science and technology of undulators and wigglers*, 4 (Oxford University Press on Demand, 2004).

[25] K.-J. Kim, Analysis of optical stochastic cooling including transverse effects, in *Proc. 16th Particle Accelerator Conference, Dallas, Texas, 1-5 May 1995*, Vol. 4 (IEEE, 1995) pp. 2786–2788.

[26] E. L. Saldin, E. A. Schneidmiller, and M. Yurkov, Statistical properties of radiation from VUV and X-ray free electron laser, Opt. Commun. **148**, 383 (1998).

[27] S. O. Rice, Mathematical analysis of random noise, Bell Syst. Tech. J. **23**, 282 (1944).

[28] Z. Huang and K.-J. Kim, Review of x-ray free-electron laser theory, Phys. Rev. ST Accel. Beams **10**, 034801

(2007).
[29] S. Gottschalk, R. Kelly, M. Offenbacker, and J. Zumdieck, Design and performance of the NLCTA-Echo 7 undulators, in *Proc. 34th International Free-Electron Laser Conference, Nara, Japan, 26-31 Aug. 2012*.
[30] O. Chubar, A. Fluerasu, L. Berman, K. Kaznatcheev, and L. Wiegart, Wavefront propagation simulations for beamlines and experiments with" synchrotron radiation workshop", in *J. Phys. Conf. Ser.*, Vol. 425 (IOP Publishing, 2013) p. 162001.
[31] Specifications of the InGaAs PIN photodiode G11193-10R on the Hamamatsu website, `https://www.hamamatsu.com/us/en/product/type/G11193-10R/index.html`, accessed: 2019-09-10.
[32] J. O. Smith, *Physical audio signal processing: For virtual musical instruments and audio effects* (W3K publishing, 2010).
[33] A. W. Chao, K. H. Mess, *et al.*, *Handbook of accelerator physics and engineering* (World scientific, 2013).
[34] M. Reiserand P. O'Shea, *Theory and design of charged particle beams*, Vol. 312 (Wiley Online Library, 1994).
[35] J. Haissinski, Exact longitudinal equilibrium distribution of stored electrons in the presence of self-fields, Il Nuovo Cimento B (1971-1996) **18**, 72 (1973).
[36] S. Nagaitsev, Intrabeam scattering formulas for fast numerical evaluation, Phys. Rev. ST Accel. Beams **8**, 064403 (2005).
[37] S.-Y. Lee, *Accelerator physics* (World Scientific Publishing, 2018).
[38] K. L. Bane, H. Hayano, K. Kubo, T. Naito, T. Okugi, and J. Urakawa, Intrabeam scattering analysis of measurements at keks accelerator test facility damping ring, Phys. Rev. ST Accel. Beams **5**, 084403 (2002).